Moon–Grazing Stable Retrograde Periodic Orbit around the Earth

Kenta Oshima (Hiroshima Institute of Technology)

Abstract

Cislunar space has been attracting interest as a strategic place to connect the Earth and interplanetary space. The present paper highlights a stable retrograde periodic orbit around the Earth as a novel option for staging orbits in cislunar space. Since the periodic orbit is linearly stable against solar gravitational perturbations, long–term operations would be more suitable than unstable orbits. The Moon–grazing geometry leads to a narrow stability region allowing modest Δv to capture into (escape from) the periodic orbit via a lunar flyby. In the analysis of capture trajectories, we globally search for transfer trajectories from the vicinity of the Earth. It is found that Sun–perturbed, multi–revolutional transfer is a promising option to reduce the launch energy and insertion Δv. In the escape analysis, the flexibility of tuning escape directions from the periodic orbit toward interplanetary space is studied. Assuming that a powered Earth flyby is a means to tune the escape energy, it is demonstrated that practical Δv and time–of–flight are able to make the escape direction arbitrary.

月近傍を通過する地球まわりの安定な逆行周期軌道

大島健太 (広島工業大学)

摘要

近年，シスルナ空間は地球と深宇宙を中継する重要拠点として注目を集めている．本研究では，シスルナ空間における新たな中継軌道の選択肢として，地球まわりの安定な逆行周期軌道に着目した．対象とした逆行周期軌道は太陽重力の摂動下においても線形安定であり，中継軌道上に長期滞在するミッションを実施する際，不安定な軌道と比較して有利であると考えられる．また，この周期軌道は月近傍を通過し安定領域が狭いことから，月スイングバイを介して十分小さい Δv によって出入りが可能である．地球近傍から逆行周期軌道への遷移軌道を大域的に探索した結果，太陽重力の摂動を利用して探査機の軌道を逆行軌道に変換した後，周期軌道の近傍において投入前に複数周回することで，打ち上げエネルギーおよび投入 Δv を低減できることがわかった．逆行周期軌道から深宇宙への脱出軌道の解析においては，パワード地球スイングバイによって脱出エネルギーを調整し，実用的な Δv と遷移時間によって脱出方向を任意に調整できることを示す．

1 Introduction

Libration point orbits and distant retrograde orbits in the Earth–Moon system have been candidate staging orbits in cislunar space connecting the Earth and interplanetary space [1, 2]. These low–energy prograde orbits around the Earth may be also useful for lunar exploration due to their low relative velocity with respect to the Moon [3]. To efficiently escape toward a distant place beyond the Moon via Earth or lunar flybys, the low–energy orbit should be converted into a high–energy trajectory in the end, such as a retrograde escape trajectory [4, 5, 6, 7, 8]. Although a low–energy escape from the Earth's gravity well is possible via the natural connection between manifolds of Earth–Moon and Sun–Earth libration point orbits [9], the resultant low–energy escape trajectories are doomed to be bounded around the Earth's orbit due to the disconnection between manifolds of Sun–Earth and Sun–planet libration point orbits [10]. In this context, an already energetic retrograde orbit around the Earth, which can skip a process of pumping up the energy in the escape phase, could be an alternative option for cislunar staging orbits toward interplanetary space.

Our previous work [11] has preliminarily investigated the accessibility of a weakly unstable retrograde periodic orbit (RPO) from the Earth and toward interplanetary space. Still, there may be capable of improvement especially in the escape analysis, which assumed that a lunar flyby is a means to increase the escape energy after departing from the RPO of relatively long period (approximately 27 days). Since an upper bound of the attainable escape energy via lunar flybys exists [5], other options such as a powered Earth flyby would expand the reachable area. Also, a longer–period staging orbit may penalize the escape energy more harshly due to its longer interval of repeating the same geometry. For example, many Earth–Mars missions have implemented approximately 21–day launch periods [12] encouraging the use of shorter–period staging orbits. Although the instability of periodic orbits may save insertion and departure Δv, the unstable nature of the RPO would not be ideal for long–term operations.

The present study deals with these issues by exploring a shorter–period (approximately 14.8 days), linearly stable RPO belonging to another family "A_1" [13]. The RPO is linearly stable in the Earth–Moon circular restricted three–body problem (CR3BP), but the linear stability assessed in the bicircular restricted four–body problem (BCR4BP) under solar gravitational perturbations can be altered even in cislunar space [14]. Section 2 introduces the CR3BP and BCR4BP and Section 3 computes RPOs in both of the models. Two RPOs of the selected synodic resonance are converged in the BCR4BP; one is linearly stable and the other is weakly unstable. Section 4 explores stability regions around each of the converged RPOs in the BCR4BP to highlight the favorable property of the linearly

stable one. Based on the result, Section 5 investigates transfer trajectory options from the vicinity of the Earth to the linearly stable RPO. Section 6 presents an analysis of escape trajectories arbitrarily tuning the escape energy via a powered Earth flyby and the escape direction by patching RPOs with practical Δv and time–of–flight.

2 Dynamical Models

To incorporate solar gravitational perturbations into RPOs (Section 3), assess the long–term stability (Section 4), or exploit solar gravitational perturbations (Section 5), we use the planar BCR4BP modeling the motion of a spacecraft under gravitational influences of the Earth, Moon, and Sun [15]. The model assumes that the Earth and Moon move on circular orbits around their barycenter and the Sun and the Earth–Moon barycenter move on circular orbits around their common barycenter in the inertial frame.

The non–dimensional equations of motion in the Earth–Moon rotating frame are [16]

$$\begin{aligned} \ddot{x} - 2\dot{y} &= -\partial \bar{U}_{4BP}/\partial x, \\ \ddot{y} + 2\dot{x} &= -\partial \bar{U}_{4BP}/\partial y, \end{aligned} \tag{1}$$

where

$$\bar{U}_{4BP} = \bar{U}_{3BP} - \frac{\epsilon m_S}{r_3} + \frac{\epsilon m_S}{a_S^2}(x\cos\theta_S + y\sin\theta_S), \tag{2}$$

$$\bar{U}_{3BP} = -\frac{1}{2}(x^2+y^2) - \frac{1-\mu}{r_1} - \frac{\mu}{r_2} - \frac{1}{2}\mu(1-\mu), \tag{3}$$

$$\begin{aligned} r_1 &= \sqrt{(x+\mu)^2 + y^2}, \\ r_2 &= \sqrt{(x-1+\mu)^2 + y^2}, \\ r_3 &= \sqrt{(x - a_S\cos\theta_S)^2 + (y - a_S\sin\theta_S)^2}, \end{aligned} \tag{4}$$

$$\theta_S = \theta_{S0} + \omega_S t, \tag{5}$$

and $\epsilon = 1$ in the BCR4BP. We also use v_x and v_y instead of $\dot{x}$ and $\dot{y}$, respectively, to represent the velocity components. The present study sets the minimum Earth flyby altitude 300 km and the minimum lunar flyby altitude 100 km.

Note that we explicitly introduce the continuous parameter ϵ to highlight the relationship between the BCR4BP and CR3BP. Substituting $\epsilon = 0$ yields equations of motion in the CR3BP. This relationship is exploited to compute periodic orbits in the BCR4BP via the continuation procedure in Section 3. In this paper, the planar CR3BP is used to simplify the analyses in Sections 3 and 6 based on its time–independent property.

3 Retrograde Periodic Orbits

This section summarizes the family A_1 [13] computed in the Earth–Moon planar CR3BP and translates an orbit of interest to the BCR4BP dynamics.

3.1 RPOs in Planar CR3BP

Figure 1 presents (a) sample orbits and (b) a characteristic curve colored according to the maximum absolute value among four eigenvalues of the monodromy matrix [16] of the family A_1 computed in the Earth–Moon planar CR3BP. The 2 : 1 synodic resonance such that a spacecraft revolves twice on the orbit while the Sun revolves once in the Earth–Moon rotating frame with the period $T_S = |2\pi/\omega_S|$ is highlighted. The definition of the 2 : 1 synodic resonance leads to the doubly revolutional geometry in the Earth–Moon rotating frame once converged in the BCR4BP.

Note that synodic resonant orbits in the CR3BP could be good initial guesses for periodic orbits in the BCR4BP due to the resonant relationship with the Sun's orbital motion in the Earth–Moon rotating frame. Among infinitely many resonances, the 2 : 1 synodic resonance is selected because of its linear stability, the tolerable period (approximately 14.8 days), and the low perilune altitude (approximately 11000 km) indicating a narrow stability region, which may allow modest Δv to capture into (escape from) the RPO via a lunar flyby.

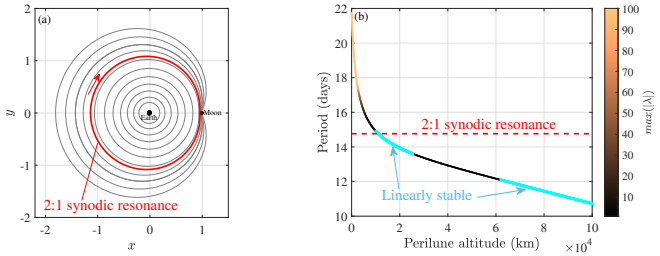

Figure 1: The family A_1 of the RPO computed in the Earth–Moon planar CR3BP.

3.2 RPOs in Planar BCR4BP

We make the 2 : 1 synodic resonant RPO in Figure 1(a) converge into periodic orbits in the BCR4BP based on the procedure developed in our recent work [17]. The symmetry in the planar BCR4BP implies the existence of two families for every synodic resonance. When M is even and N is odd for a certain $M : N$ synodic resonance, there exist "left" and "right" families. One can constrain initial states of left and right families at $y = v_x = 0$ with smaller and larger values of x, respectively, with the initial solar phase angle $\theta_{S0} = 0$ to efficiently compute periodic orbits along a continuation process from $\epsilon = 0$ (CR3BP) to $\epsilon = 1$ (BCR4BP). See Ref. [17] for details.

Figure 2 shows the evolution of (a) the initial value of x and (b) the absolute value of each of four eigenvalues of the monodromy matrix in terms of ϵ along the continuation pathways. As the name of the families indicates, the initial value of x at $y = v_x = 0$ with $\theta_{S0} = 0$ is smaller for the left family. Note also that the almost constant evolution of x along the continuation pathways implies that the geometry of the 2 : 1 synodic resonant RPOs of both families is hardly affected by solar gravitational perturbations. On the other hand, the panel (b) highlights that the instability arises only in the left family once the solar gravitational effect is turned on.

Figure 3 (a) presents the 2 : 1 synodic resonant RPOs of the left (broken curve) and right (solid curve) families converged in the BCR4BP ($\epsilon = 1$). Although the difference in the position space is somehow visible, Figure 3 (b) clarifies the difference by plotting x and θ_S at $y = 0$. The solar phase angle is expressed between 0 and 2π by the modulo operation. Two apolune states (#1 and #2) for each of the families, the position and velocity of which are varied in the next sections, are indicated. Note that the panel (b) also highlights the doubly revolutional geometry of the orbits implied from the definition of the 2 : 1 synodic resonance in Section 3.1.

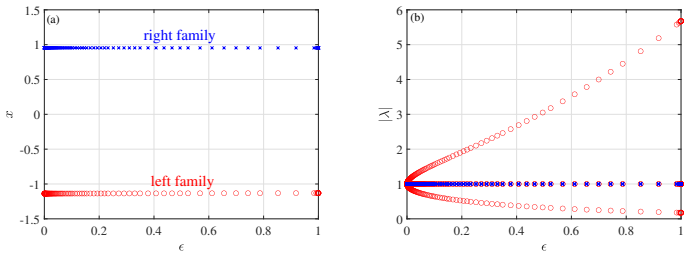

Figure 2: The continuation pathways from the CR3BP ($\epsilon = 0$) to the BCR4BP ($\epsilon = 1$) of the left (cross) and right (circle) families of the 2 : 1 synodic resonant RPO.

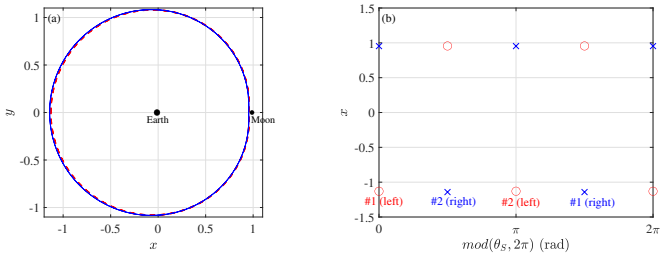

Figure 3: The 2 : 1 synodic resonant RPOs of the left (red) and right (blue) families in the BCR4BP.

4 Stability Regions

This section explores stability regions around the 2 : 1 synodic resonant RPOs of the left and right families in Figure 3. We give a position (Δx and Δy) or velocity (Δv_x and Δv_y) error on the two apolune states (#1 and #2) for each of the families and propagate the perturbed states for 200 days in the planar BCR4BP. We stop propagations if one of the following escape conditions is satisfied: a trajectory violates $0.9 < r_1 < 1.2$, i.e., it is far from the RPO; a trajectory violates the minimum lunar flyby altitude.

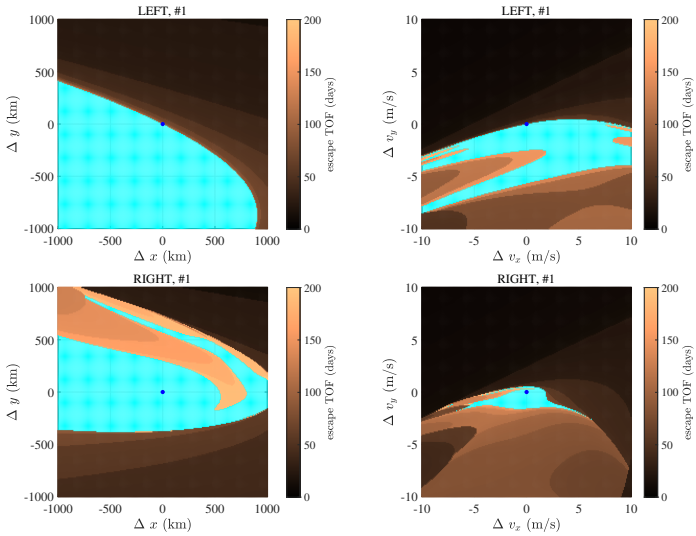

Figure 4: Stability regions (cyan) around the 2 : 1 synodic resonant RPOs (blue dot on the origin) of the left (top panels) and right (bottom panels) families in the planar BCR4BP.

Figure 4 exhibits the stability regions around the 2 : 1 synodic resonant RPOs. The color indicates the time–of–flight (TOF) until one of the escape conditions is satisfied. The results of the other apolune #2 are omitted because they are almost indistinguishable from those of #1. Since the left family is unstable, it is located on the stability boundary. On the other hand, the right family is surrounded by the stability region and thus it may be more robust against disturbances. Note also that modest Δv allows a spacecraft to capture into (escape from) the right family across its narrow stability region. This is the reason we give priority to th right family and further investigate transfer trajectories into it from the vicinity of the Earth in the next section.

5 Capture Analysis

This section investigates transfer options from the vicinity of the Earth into the right family of the 2 : 1 synodic resonant RPO. We assume an impulsive maneuver at the apolune states #1 or #2, i.e., insertion Δv, and propagate the perturbed states backward in time for 200 days in the planar BCR4BP. Once a trajectory reaches 10000 km altitude from the Earth as a prograde orbit, we evaluate TOF and C_3 [12]. We stop propagations if a trajectory violates one of the minimum flyby altitudes. The method is similar to the one in Ref. [11], but the periodic orbit family of interest is different and the evaluation of insertion Δv is more accurate because the periodic orbit is computed in the BCR4BP in the present paper.

Figure 5 shows the values of TOF, C_3, and insertion Δv for transfer trajectories into the apolunes #1 and #2 of the right family of the 2 : 1 synodic resonant RPO. The nearly π difference in the solar phase angles at the apolunes in Figure 3 (b) leads to the similar solution structures. Four sample solutions with small C_3 and insertion Δv are indicated to study mechanisms for reducing them.

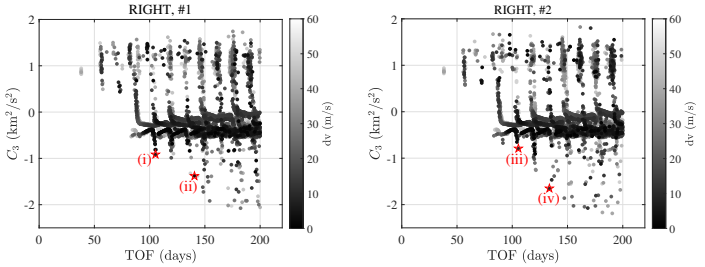

Figure 5: Transfer options from the vicinity of the Earth into the apolunes #1 (left panel) and #2 (right panel) of the right family of the 2 : 1 synodic resonant RPO.

Figures 6 and 7 present transfer trajectories of the sample solutions (i) and (ii) into the apolune #1 and (iii) and (iv) into the apolune #2, respectively. We highlight two common characteristics among the four sample solutions. The additional revolution around the RPO before the insertion that is clear in the amplified figures in the middle column is useful for reducing insertion Δv. We confirm that direct insertions appear for solutions with larger insertion Δv. The placement of an apogee in the first or third quadrant around the Earth as those in the right column reduces the angular momentum of a trajectory [18] and sometimes converts it into a retrograde one [4], which also contributes to the reduction of insertion Δv into the RPO. Note that the nearly π difference in the solar phase angles at the apolunes #1 and #2 results in the almost opposite placement of the apogees in Figures 6 and 7. If a lunar flyby is adopted, the use of solar gravitational perturbations is available for trajectories launched with the energy enough for reaching the lunar orbit and thus the Sun–perturbed option reduces C_3

down to the level of standard lunar transfers [19] at the cost of substantial TOF typical for low–energy lunar transfers [20].

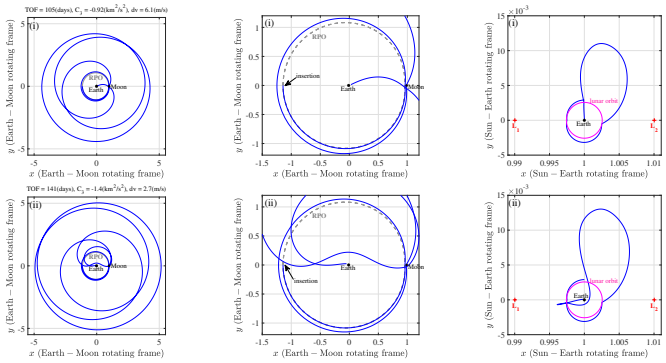

Figure 6: Sample capture solutions (i) and (ii).

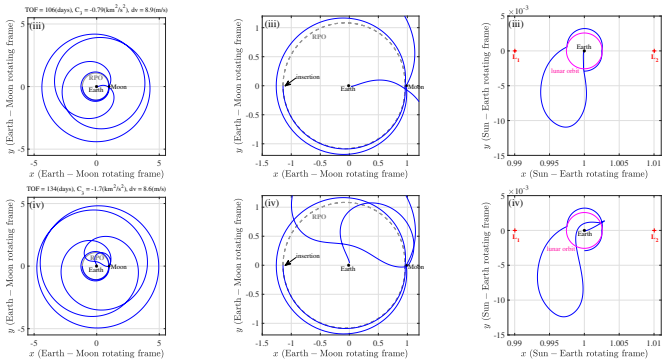

Figure 7: Sample capture solutions (iii) and (iv).

6 Escape Analysis

This section assesses the amount of Δv and TOF required to arbitrarily tune the escape direction from the 2 : 1 synodic resonant RPO of the family A_1 toward interplanetary space. Since we adopt a powered Earth flyby, the escape energy can be adjusted via the magnitude of an impulsive maneuver at perigee.

6.1 Escape Direction

This subsection defines the escape direction before computing escape trajectories. Let $\boldsymbol{v}_\infty^{out}$ be the outgoing hyperbolic excess velocity vector with respect to the Earth, θ_{out} be the angle between $\boldsymbol{v}_\infty^{out}$ and an X–axis in the Earth–centered inertial frame, and θ_S^{Ein} be the angle between the Earth–Sun line and the X–axis as illustrated in Figure 8. We then use the angle

$$\theta_{esc} = \theta_{out} - \theta_S^{Ein} \tag{6}$$

to uniquely define the escape direction toward a target body.

It is convenient to rewrite Eq. (6) via parameters used in the Earth–Moon rotating frame. Assuming that the x–axis in the Earth–Moon rotating frame and the X–axis in the Earth–centered inertial frame coincide at $t = 0$ and time at a powered Earth flyby is $t = t_{PG}$. Substituting $t = t_{PG}$ into Eq. (5) yields the solar phase angle

$$\theta_{S_{PG}} = \theta_{S0} + \omega_S t_{PG}, \tag{7}$$

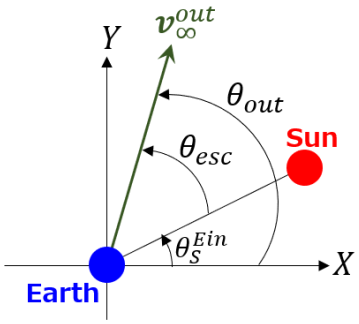

Figure 8: The definition of θ_{esc} denoting the escape direction.

and correspondingly the Sun's location at a powered Earth flyby in the Earth–Moon rotating frame

$$\begin{aligned} x_{S_{PG}} &= a_S \cos\theta_{S_{PG}}, \\ y_{S_{PG}} &= a_S \sin\theta_{S_{PG}}. \end{aligned} \tag{8}$$

Transforming Eq. (8) into the Earth–centered inertial frame [21] yields

$$\begin{aligned} x_{S_{PG}}^{Ein} &= (x_{S_{PG}} + \mu)\cos t_{PG} - y_{S_{PG}} \sin t_{PG}, \\ y_{S_{PG}}^{Ein} &= (x_{S_{PG}} + \mu)\sin t_{PG} + y_{S_{PG}} \cos t_{PG}. \end{aligned} \tag{9}$$

One may further rewrite Eq. (9) by substituting Eq. (8) as

$$\begin{aligned} x_{S_{PG}}^{Ein} &= \mu\cos t_{PG} + a_S \cos(\theta_{S_{PG}} + t_{PG}), \\ y_{S_{PG}}^{Ein} &= \mu\sin t_{PG} + a_S \sin(\theta_{S_{PG}} + t_{PG}). \end{aligned} \tag{10}$$

Thus, θ_S^{Ein} at a powered Earth flyby can be expressed as

$$\tan\theta_{S_{PG}}^{Ein} = \frac{\mu\sin t_{PG} + a_S \sin(\theta_{S_{PG}} + t_{PG})}{\mu\cos t_{PG} + a_S \cos(\theta_{S_{PG}} + t_{PG})}, \tag{11}$$

which may be converted into a simpler form by composing the trigonometric functions

$$\tan\theta_{S_{PG}}^{Ein} = \tan(\theta + \phi), \tag{12}$$

or

$$\theta_{S_{PG}}^{Ein} = \theta + \phi, \tag{13}$$

where

$$\theta = t_{PG} + \frac{\theta_{S_{PG}}}{2}, \tag{14}$$

$$\tan\phi = \frac{a_S - \mu}{a_S + \mu}\tan\frac{\theta_{S_{PG}}}{2} \approx \tan\frac{\theta_{S_{PG}}}{2}, \tag{15}$$

leading to

$$\phi \approx \frac{\theta_{S_{PG}}}{2}. \tag{16}$$

Substituting Eq. (14) and Eq. (16) into Eq. (13) yields

$$\theta_{S_{PG}}^{Ein} \approx \theta_{S_{PG}} + t_{PG}, \tag{17}$$

and using Eq. (7) results in

$$\theta_{S_{PG}}^{Ein} \approx \theta_{S0} + (1 + \omega_S)t_{PG}. \tag{18}$$

Therefore, the escape direction in Eq. (6) can be approximated as

$$\theta_{esc} \approx \theta_{out} - \theta_{S0} - (1 + \omega_S)t_{PG}. \tag{19}$$

Note that θ_{S0} is an epoch–dependent constant and thus one can evaluate the ability of arbitrarily tuning the escape direction based on the maximum Δv and TOF required to cover the whole range of

$$\theta'_{esc} = \theta_{out} - (1 + \omega_S)t_{PG}, \tag{20}$$

which is independent of the Sun's location. This leads to the simplification of the analysis on escape trajectories by adopting the time–independent Earth–Moon planar CR3BP. Since the RPO is a high–energy orbit, capture trajectories require the use of solar gravitational perturbations in Section 5, but escape trajectories from the already energetic RPO does not need to exploit them.

6.2 Escape Trajectories

Eq. (20) indicates that the escape direction can be tuned not only by changing the position and velocity at perigee but also by varying time at perigee. Therefore, we adopt a strategy of patching RPOs of two different families to leverage various periods and geometries. One family is A_1 [13] in Figure 1 that the initial $2:1$ synodic resonant orbit belongs to, and the other is the family I [17], to which the initial $2:1$ orbit can be connected with small Δv. The computation of escape trajectories from the $2:1$ synodic resonant RPO of the family A_1 consists of the following procedure:

1. Give an impulsive maneuver (Δv_1) at apolune of the initial orbit and propagate the perturbed states forward in time for the quadruple of the period (approximately 59 days). Store the orbital data when crossing $y = 0$ with $v_y > 0$ and stop propagations if a trajectory violates one of the minimum flyby altitudes. Figure 9 (a) shows the values of x at $y = 0$ with $v_y > 0$ in terms of Δv_1 and TOF.

2. At every intersection with $y = 0$ and $v_y > 0$, find the nearest apolune position among each of the RPO families, make the RPOs cross the intersection point via the shooting procedure, and compute the insertion maneuver (Δv_2). Figure 9 (b) and (c) present TOF in terms of the period of the inserted RPOs and Δv_2 for the families A_1 and I, respectively.

3. Give an impulsive maneuver (Δv_3) on the inserted state and minimize Δv_3 such that the trajectory reaches perigee at 1000 km altitude from the Earth via the multiple shooting procedure [22].

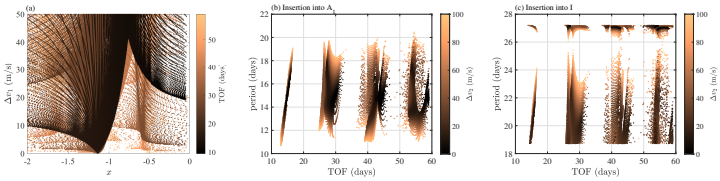

Figure 9: Computational procedure of escape trajectories.

Since the variation of time at perigee affects the escape direction, it may be meaningful to incorporate additional revolutions on the initial $2:1$ RPO and the inserted RPO into every converged zero–revolutional solution in the step 3. We set the maximum numbers of revolutions one on the initial $2:1$ RPO, four on the inserted RPO of the family A_1, and three on the inserted RPO of the longer–period family I.

Note that Δv_2 and Δv_3 are merged into a single maneuver in the cases of zero revolution on inserted RPOs. It is straightforward to derive the magnitude of a tangential perigee maneuver Δv_{PG} producing the desired change in the escape energy ΔC_3 as

$$\Delta v_{PG} = -V_{PG} + \sqrt{{V_{PG}}^2 + \Delta C_3}, \tag{21}$$

where V_{PG} is the magnitude of the velocity at perigee in the Earth–centered inertial frame.

Figure 10 shows resultant θ'_{esc} and total Δv of escape solutions with total TOF less than 80 days, for example, until reaching perigee. The panels (a) and (b) correspond to the results before and after executing Δv_{PG} to attain $C_3 = 10$ (km^2/s^2), respectively. The execution of Δv_{PG} slightly changes $\boldsymbol{v}_\infty^{out}$ and thus varies θ'_{esc}. The difference between the panels corresponding to $\Delta v_{PG} \approx 440$ m/s is in accordance with the perigee maneuver in the planned escape trajectory of Nozomi toward Mars [4, 5]. Figure 10 (a) indicates that total Δv of approximately 50 m/s at most attains arbitrary escape directions within 80 days.

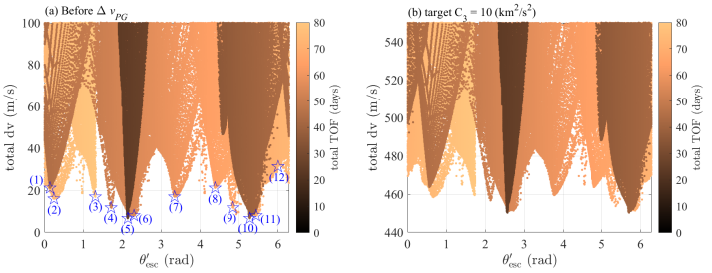

Figure 10: Escape solutions with total TOF less than 80 days.

Figure 11 exhibits the sample escape trajectories in the Earth–centered inertial frame indicated in Figure 10 (a). The color distinguishes the phases of revolution on the initial RPO (magenta), transfer into different RPOs (dark green), revolution on inserted RPOs (red), and transfer into perigee (blue). All of the trajectories enjoy a close approach to the Moon (broken curve) en route to perigee. The insertion into the family I is a favorite option adopted in the samples (1), (2), (3), (7), and (8) experiencing the relatively low perigee altitudes during the revolutional phase. The use of the family A_1 appears in the revolutional phase on inserted RPOs in the sample (12) as well as the phase of revolution on the initial RPO in the samples (9), (10), and (11). Note that transfers with revolutions on neither the initial RPO nor inserted RPOs are also potential options found in the samples (4), (5), and (6).

7 Conclusion

The present paper has explored orbital characteristics of the retrograde periodic orbit (RPO) around the Earth influential in the usefulness as a staging orbit toward interplanetary space. Firstly, we have found a linearly stable RPO under solar gravitational perturbations with the tolerable period of approximately 14.8 days. The narrow stability region around the RPO would aid long–term operations as well as contributes to the modest insertion (departure) Δv. This is beneficial to transfer trajectories from the vicinity of the Earth for reducing the critical insertion maneuver down to Δv less than 10 m/s. The combination with the use of solar gravitational perturbations leads to comparable costs with typical low–energy transfers into

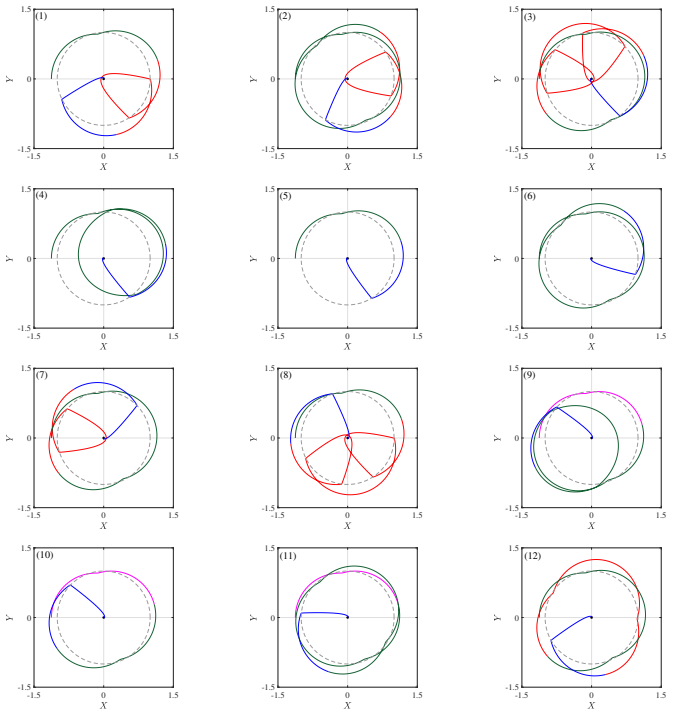

Figure 11: Sample escape trajectories in the Earth–centered inertial frame.

cislunar libration point orbits. The analysis on escape trajectories from the RPO has found that arbitrary escape directions are achievable with Δv of approximately 50 m/s at most within 80 days until reaching perigee. The strategy of exploiting a powered Earth flyby is able to tune the escape energy via the maneuver at perigee, the magnitude of which has been confirmed to be in accordance with a prior mission.

Acknowledgments

The author is grateful to the valuable comments and suggestions from Dr. Yuichi Tsuda, Dr. Takanao Saiki, and Dr. Yuto Takei in ISAS/JAXA. This study has been partially supported by JSPS Grants–in–Aid No.20K14951.

References

[1] Kakoi, M., Howell, K. C., and Folta, D., "Access to Mars from Earth–Moon Libration Point Orbits: Manifold and Direct Options," *Acta Astronautica*, Vol. 102, 2014, pp. 269–286. http://dx.doi.org/10.1016/j.actaastro.2014.06.010.

[2] Conte, D., Di Carlo, M., Ho, K., Spencer, D. B., and Vasile, M., "Earth–Mars Transfers through Moon Distant Retrograde Orbits," *Acta Astronautica*, Vol. 143, 2018, pp. 372–379. https://doi.org/10.1016/j.actaastro.2017.12.007.

[3] Whitley, R. and Martinez, R., "Options for Staging Orbits in Cislunar Space," *IEEE Aerospace Conference*, Big Sky, Mar. 2016.

[4] Kawaguchi, J., Yamakawa, H., Uesugi, T., and Matsuo, H., "On Making Use of Lunar and Solar Gravity Assists in Lunar–A, Planet–B Missions," *Acta Astronautica*, Vol. 35, 1995, pp. 633–642. https://doi.org/10.1016/0094-5765(95)00013-P.

[5] McElrath, T. P., Lantoine, G., Landau, D., Grebow, D., Strange, N., Wilson, R., and Sims, J., "Using Gravity Assists in the Earth–Moon System as a Gateway to the Solar System," *Global Space Exploration Conference*, Washington, D. C., May. 2012.

[6] Lantoine, G. and McElrath, T. P., "Families of Solar–Perturbed Moon–to–Moon Transfers," *24th AAS/AIAA Spaceflight Mechanics Meeting*, Santa Fe, Jan. 2014.

[7] Yárnoz, D. G., Yam, C. H., Campagnola, S., and Kawakatsu, Y., "Extended Tisserand–Poincaré Graph and Multiple Lunar Swingby Design with Sun Perturbation," *6th International Conference on Astrodynamics Tools and Techniques*, Darmstadtium, Mar. 2016.

[8] Suda, S., Kawakatsu, Y., Sawai, S., Nagata, H., and Totani, T., "Orbit Manipulation by Use of Lunar Swing–By on a Hyperbolic Trajectory," *26th AAS/AIAA Spaceflight Mechanics Meeting*, San Antonio, Feb. 2017.

[9] Koon, W. S., Lo, M. W., Marsden, J. E., and Ross, S. D., "Low Energy Transfer to the Moon", *Celestial Mechanics and Dynamical Astronomy*, Vol. 81, 2001, pp. 63–73. https://doi.org/10.1023/A:1013359120468.

[10] Ren, Y., Masdemont, J. J., Gómez, G., and Fantino, E., "Two Mechanisms of Natural Transport in the Solar System," *Communications in Nonlinear Science and Numerical Simulation*, Vol. 17, 2012, pp. 844–853. https://doi.org/10.1016/j.cnsns.2011.06.030.

[11] Oshima, K., "Capture and Escape Analyses on Planar Retrograde Periodic Orbit around the Earth," *Advances in Space Research*, Vol. 68, 2021, pp. 3891–3902. https://doi.org/10.1016/j.asr.2021.07.012.

[12] Vallado, D. A., *Fundamentals of Astrodynamics and Applications*, Microcosm Press, Hawthorne, 2013.

[13] Broucke, R. A., "Periodic Orbits in the Restricted Three–Body Problem with Earth–Moon Masses," *JPL Technical Report*, 32–1168, 1968.

[14] Boudad, K. K., Howell, K. C., and Davis, D. C., "Dynamics of Synodic Resonant Near Rectilinear Halo Orbits in the Bicircular Four–Body Problem," *Advances in Space Research*, Vol. 66, 2020, pp. 2194–2294. https://doi.org/10.1016/j.asr.2020.07.044.

[15] Simó, C., Gómez, G., Jorba, À., and Masdemont, J., "The Bicircular Model near the Triangular Libration Points of the RTBP," *In: Roy, A. E., Steves, B. A. (ed.) From Newton to Chaos*, Springer, Boston, 1995.

[16] Koon, W. S., Lo, M. W., Marsden, J. E., and Ross, S. D., *Dynamical Systems, the Three–Body Problem and Space Mission Design*, Marsden Books, Wellington, 2011.

[17] Oshima, K., "Continuation and Stationkeeping Analyses on Planar Retrograde Periodic Orbits around the Earth," submitted.

[18] Miller, J. K., "Lunar Transfer Trajectory Design and the Four Body Problem," *13th AAS/AIAA Spaceflight Mechanics Meeting*, Ponce, Feb. 2003.

[19] Parker, J. S. and Anderson, R. L., *Low–Energy Lunar Trajectory Design*, John Wiley & Sons, Hoboken, 2014.

[20] Belbruno, E. and Miller, J., "Sun–Perturbed Earth–to–Moon Transfers with Ballistic Capture," *Journal of Guidance, Control, and Dynamics*, Vol. 16, 1993, pp. 770–775. https://doi.org/10.2514/3.21079.

[21] Topputo, F., "On Optimal Two–Impulse Earth–Moon Transfers in a Four–Body Model", *Celestial Mechanics and Dynamical Astronomy*, Vol. 117, 2013, pp. 279–313. https://doi.org/10.1007/s10569-013-9513-8.

[22] Betts, J. T., "Survey of Numerical Methods for Trajectory Optimization," *Journal of Guidance, Control, and Dynamics*, Vol. 21, 1998, pp. 193–207. http://dx.doi.org/10.2514/2.4231.